Chemical Physics Letters 539–540 (2012) 94–101

Contents lists available at SciVerse ScienceDirect

Chemical Physics Letters

journal homepage: www.elsevier.com/locate/cplett

Hybrid C-nanotubes/Si 3D nanostructures by one-step growth in a dual-plasma reactor

Francesco Toschi [a], Silvia Orlanducci [a], Valeria Guglielmotti [a], Ilaria Cianchetta [a], Corrado Magni [a], Maria Letizia Terranova [a], Matteo Pasquali [b], Emanuela Tamburri [a,b], Roberto Matassa [c], Marco Rossi [c,*]

[a] Department of Science and Chemical Technologies and Micro and Nano-structured Systems (MINAS) Lab, University of Rome 'Tor Vergata', Via della Ricerca Scientifica 1, 00133 Roma, Italy
[b] Chemical and Biomolecular Engineering Dept., Rice University, P.O. Box 1892, Houston, TX 77251-1892, USA
[c] Department of Fundamental and Applied Sciences for Engineering and Research Center of Nanotechnologies for Engineering (CNIS), University of Rome 'La Sapienza', Via A. Scarpa 14, 00161 Roma, Italy

ARTICLE INFO

Article history:
Received 20 February 2012
In final form 1 May 2012
Available online 9 May 2012

ABSTRACT

Hybrid nanostructures consisting of Si polycrystalline nanocones, with an anemone-like termination coated with C-nanotubes bundles, have been generated on a (100) Si substrate in a dual mode microwave/radio-frequency plasma reactor.

The substrate is both heated and bombarded by energetic H ions during the synthesis process. The nanocones growth is explained considering pull of the growing Si nanocrystalline phase along the lines of the electrical field, likely via a molten/recrystallization mechanism. The one-step building of the achieved complex 3D architectures is described in terms of dynamic competition between Si and C nanotubes growth under the peculiar conditions of kinetically driven processes.

1. Introduction

The current impact of nanocrystalline structures made from C and Si, the lightest atomic weight elements of the IV group of the Periodic Table, is enormous, considering that their potential technological impact does not require significant investment, because they are compatible with the current Si technology [1–5].

These elements are indeed particularly suitable for the realization of zero-dimensional (0D) and one-dimensional (1D) structures with interesting and unexpected opto-electronic properties. In these nanosized systems the physical properties are strongly affected by the local confinement of the electrons giving rise to phenomena that are not revealed in systems formed by the same materials but with micrometric size.

C-nanotubes, nanofibers, nanoparticles, as well as Si quantum dots, nanoparticles and nanowires, are fundamental and versatile building blocks for the fabrication of hybrid devices for a variety of technology applications. As an example, FET have been configured from Si nanowires and C-nanotubes [1] and nanostructured hybrid silicon/carbon nanotube heterostructures have been proposed [2] as next generation anodes exhibiting high energy density and cycle life to be used in lithium-ion batteries.

In this context it is thought that, by coupling different C and Si nanostructures, new materials characterized by novel physical properties could be obtained. As an example, nanostructures based on C-nanotubes and Si nanoparticles can be used in quantum computing technology [3,4].

However, the experimental research in the field of hybrid systems based on C and Si nanostructures remains at an early stage and many of the potential hybrids between these fourth group elements are not yet explored.

In the course of research dealing with production of C nanomaterials by CVD techniques [6–8] we noted, according to the pioneeristic results reported by a Japanese group [9,10], that, under well-defined conditions, it was possible to simultaneously generate exciting combinations of C-nanotubes and other nanostructures, such as Si nanowires and nanodiamonds. For the generation of such nanostructures, we obtained more interesting results using Plasma Enhanced Chemical Vapour Deposition (PE-CVD) reactors, in particular a dual mode microwave/radio frequency plasma system [11–14]. Indeed, as already reported, this technique connects the advantages of microwave discharge, such as homogeneity of plasma and high concentration of active chemical species, with the ability to control ion energy by proper biasing of the substrate [14], and makes it possible to obtain many different carbon materials [15].

The main goal of the present research is to determine the key macroscopic parameters for the deposition of vertically oriented arrays of crystalline Si/C systems on patterned Si substrates using a dual mode microwave/radio frequency plasma CVD technique.

* Corresponding author.
E-mail address: marcorossi@uniroma1.it (M. Rossi).

0009-2614/$ - see front matter © 2012 Elsevier B.V. All rights reserved.
http://dx.doi.org/10.1016/j.cplett.2012.05.001

2. Experimental

The samples were grown in a custom designed Plasma Enhanced Chemical Vapour Deposition (PE-CVD) reactor, where Micro Waves (MW) capacitively coupled to Radio Frequency (RF) excites the gas phase. The main components of the MW/RF CVD system are: the MW and RF generators, the water-cooled process chamber and the vacuum and gas handling systems.

The substrate holder (diameter of 120 mm), located at the center of the chamber on a cylindrical support, is integrated with a Joule-based heating system and a thermocouple.

The microwave system is positioned on the top of the chamber and is formed by three components: the MW magnetron generator (ASTEC) connected to High Voltage power supply (max power 600 W), the arc detector for detection of the reflected power during the synthesis process and the quartz tubing waveguide to collimate the MW in the process chamber. The working frequency of MW is 2.46 GHz.

The Radio Frequencies (RF) system is hosted in the bottom of the chamber. The RF power supply can provide 600 W and a frequency of 13.56 MHz. The RF system is equipped with a matching network system with adjustable coupling impedance, in order to optimize the RF Plasma and to prevent power supply damages induced by the RF reflected power. The RF power is transferred at the substrate-holder, acting also as RF antenna, by means of a RG213 cable with an impedance of 50 Ω. Setting and control of the various parts of the MW-RF reactor are integrated in a computer-controlled system.

In order to initialize the plasma, two frequencies are applied: Micro Wave (2.45 GHz) and Radio Frequency (13.56 MHz). It is worth mentioning that whereas the single MW discharge does not induce DC polarization of the substrate holder, the application of a RF plasma induces a negative bias voltage, V_b (measured with respect to the ground), in the substrate holder [11]. The V_b values represent an indirect measure of the energy due to the ions impinging on the substrate and are dependent on both the RF power and the chamber configuration. These V_b values are also strongly dependent on the working pressure of the chamber, as shown by a series of calibration tests carried out during the present research. The experiments carried out at constant RF power allowed us to establish the V_b dependence on pressure P in the range 5–50 mbar. The data of V_b vs. lnP, plotted in Figure 1, clearly show

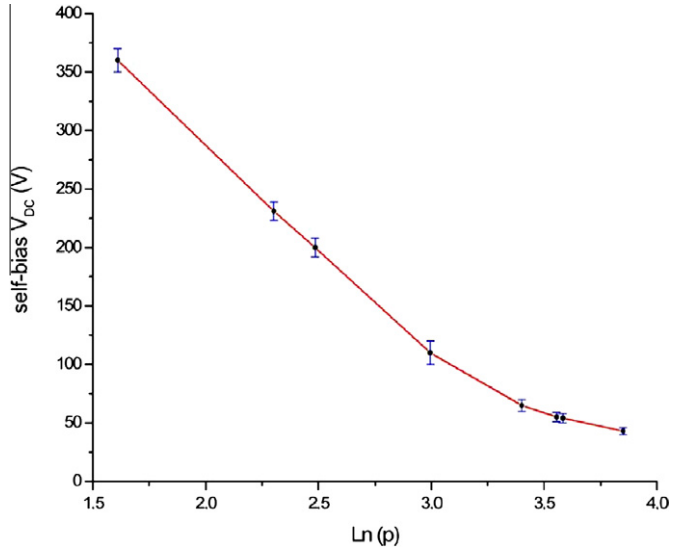

Figure 1. Plot of the measured values of self-bias voltage (V_b) as a function of lnP.

that increasing P results in a net decrease of the self-bias. Up to approximately 20 mbar there is linearity between bias (V_b) and lnP, indicating an ideal behavior of the gas phase, but at higher pressures there is an evident deviation from linearity, typical of an inelastic collisional regime.

The fit of the experimental data yields:

$$V_b = A + Be^{-CP}$$

where $A = 39 \pm 1$ V, $B = 529 \pm 1$ V and $C = 0.100 \pm 0.001$ mbar^{-1}.

From the above equation it is possible to determine the value of the biasing at any P value in the range 5–50 mbar.

The fixed parameters in the present experiments were the MW and RF powers (both 100 W), the H_2 and CH_4 fluxes (100 and 20 sccm, respectively), and the deposition times (30 min). The sample temperature, fixed at 510 ± 10 °C at the beginning of the process, was found to increase up to 620 ± 10 °C during the process. The total pressure P_{tot} was varied in the range 5–50 mbar.

On the basis of preliminary results, the two following synthesis conditions have been selected and used for the two series of runs to produce the samples discussed in this Letter.

Condition I: $P_{tot} = 35$ mbar, $V_b = 55$ V
Condition II: $P_{tot} = 10$ mbar, $V_b = 240$ V

The synthesis experiments have been carried out on lithographically patterned areas of Si (1 0 0) substrates. Some substrates were patterned with areas shaped as 'number four' in honour of the IV group elements. Other substrates were patterned with circular areas of 150 nm diameter.

A series of substrates have been prepared by sputtering thin layers (thickness: 15 nm) of the Ni catalyst inside the patterned areas. Other substrates were prepared by depositing 15 nm of TiN interlayer between the Si substrate and the Ni catalyst.

Field emission scanning electron microscopy (FE-SEM), transmission electron microscopy (TEM), transmission electron diffraction (TED), reflection high-energy electron diffraction (RHEED) and micro-Raman spectroscopy have been used for the samples characterization at the micro and nanoscale.

Conventional and high-resolution transmission electron microscopy, and diffraction analysis have been carried out on a TEM Hitachi model H-7100 and a TEM JEOL model 2010, setting the acceleration of the electron beam at 125 and 160 keV, respectively.

Specific ultrasound-based methodologies have been set-up in order to prepare the samples for the different ED and TEM analysis.

RHEED observations have been performed at 60 keV on an electron optics column AEI EM6G, equipped with a high-resolution diffraction stage.

The micro-Raman spectra were acquired using an Ar ion laser (514.5 nm excitation wavelength, 1 mW power), a 600 gr/mm and a 1800 gr/mm gratings spectrometer (iHR550 - HORIBA JOBIN YVON) coupled with a liquid-nitrogen cooled CCD. The spectral resolution is 3 cm^{-1} (using the 600 gr/mm) and lower than 1 cm^{-1} (using the 1800 gr/mm). The Raman spectra here reported have been acquired with a microscope objective of 100×, using a power density of about 0.3 mW/μm^2.

3. Results and discussion

Under condition I, deposits of entangled C nanotubes bundles were produced inside the catalyzed areas, as shown by the FE-SEM images of Figure 2a and b. Totally different deposited structures were obtained under condition II, as shown by the images reported in Figure 2c and d.

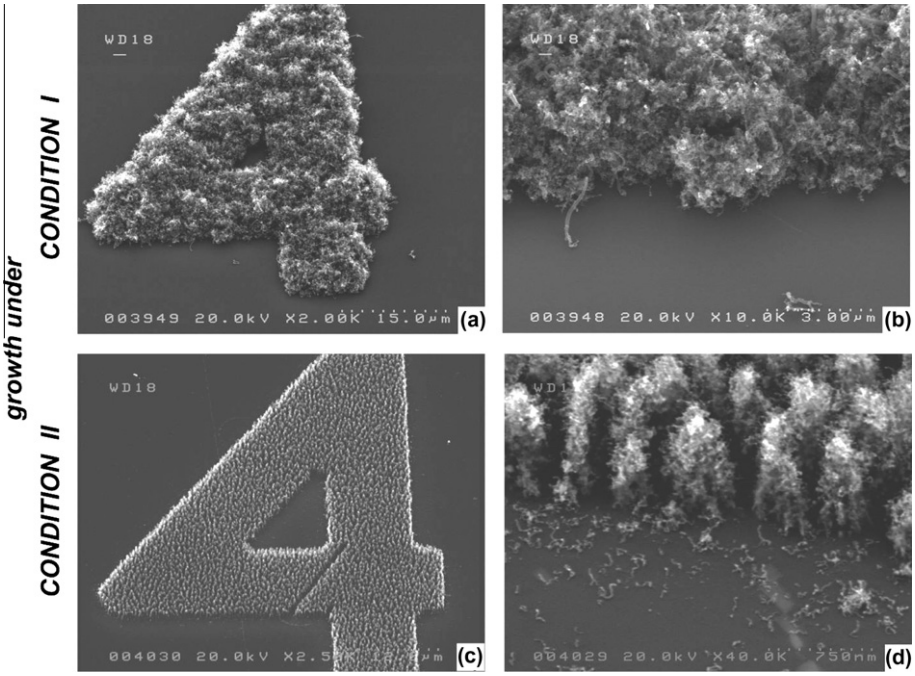

Figure 2. FE-SEM images, at moderate tilt angle of about 15°, of typical deposits grown under condition I (a–b) and condition II (c–d) on patterned Si substrates.

Condition II produced arrays of discrete deposits (length up to 1 μm) protruding from the Si substrate. The higher magnification images (see for example Figure 2d) highlight that the outermost part of such vertically elongate structures consists of randomly positioned mats of C-nanotubes bundles. The peculiar 3D arrangements of such disordered deposits of C-nanotubes suggest the presence of a possible underlying architecture that acts as a support for the nanotubes. Some bundles, likely detached from the protruding deposits, can be observed on the surface of the substrate at the boundary between the coated and uncoated areas.

The structural features of the outermost layers have been investigated *ex-situ* by reflection high-energy electron diffraction (RHEED). The high-resolution goniometer stage made it possible to carry out the RHEED analysis by varying the angle of incidence, θ, of the electron beam with respect to the specimen surface. The RHEED technique is a truly effective characterization technique in revealing fine details and modifications in the structural features of samples with a very high sensitivity. It is able to achieve structural information from very few atomic layers also at different depths by varying the angle of incidence [16], making possible to determine the stacking sequence in case of layered materials.

The roughness of the outermost deposit determined by the random entangling of C-nanotubes bundles over the substrate determined the experimental condition in which has been possible to obtain the transmission electron diffraction (TED) pattern through the top of the protruding structures reported in Figure 3a. In such conditions, the electron diffraction pattern reveals diffraction discs superimposed on some broadened diffraction rings (with intensity comparable to that of diffractions discs) that can be ascribed to the concurrent presence of Single-Walled C-nanotubes (SWCNTs) and Multi-Walled C-nanotubes (MWCNTs), respectively [17].

In order to investigate the structural properties of the surfaces underlying the C-nanotubes mats, the last ones have been removed by a suitable and selective chemical procedure aided by an ultrasound treatment. In Figure 3b the corresponding experimental RHEED pattern is reported. Its analysis (Figure 3c–d) revealed the presence of two concomitant sets of Debye's rings, one corresponding to nanocrystalline Si and the other one belonging to nanocrystalline $NiSi_2$ with a preferential orientation parallel to the substrate and having a cubic structure with a lattice constant spacing $a = 0.541$ nm [18–20]. The RHEED analysis, carried out exploiting the possibility to vary the angle of incidence of the e-beam on the sample, evidenced a very thin outermost layer of nanocrystalline $NiSi_2$ on the underlying nanocrystalline Si.

Different Ni-silicides with different stoichiometric Ni/Si ratio are known, with spatial density of the Ni atoms changing from about 70% (Ni_2Si) to about 25% ($NiSi_2$) of the bulk Ni density [20]. Under our experimental conditions, the formation of the silicide with the lowest Ni content among those seems reasonable.

A complementary insight about the structural properties of the vertical deposits has been obtained by means of Raman spectroscopy. The spectra taken from the deposits depicted in Figure 2a and c are reported in Figure 4a and b, as spectra A and spectra B, respectively. Figure 4a shows the Raman spectra in the radial breathing mode (RBM) range, evidencing the presence of characteristic signals corresponding to radial expansion-contraction of SWCNTs.

The Raman shifts in the range 400–2000 cm^{-1} are reported in Figure 4b, where both spectra show peaks at about 520 and 980 cm^{-1}, due to the first and second order vibrations of Si [21]. The broadened bands at 1350 and 1598 cm^{-1} correspond to the D and G bands, which are the typical features that characterize nanographytic structures [22]. In the spectrum taken from samples grown under condition II (Figure 4b, spectrum B) a strong luminescence is also noted. The presence of the luminescence band is likely due to small amounts of hydrogenated amorphous carbon [23] and has also been detected in other experiments of C deposition carried out employing high self-bias induced by RF [24]. Under such conditions the electrical field related to the negative self-bias is expected to interact with the hydrogen ions of the plasma, giving them a sufficient energy to induce an effective hydrogenation of the amorphous carbon produced during the CVD process.

In order to account for the rather peculiar features of the deposits obtained under condition II, we felt it worthwhile to perform a detailed analysis of the first-order Raman scattering from Si.

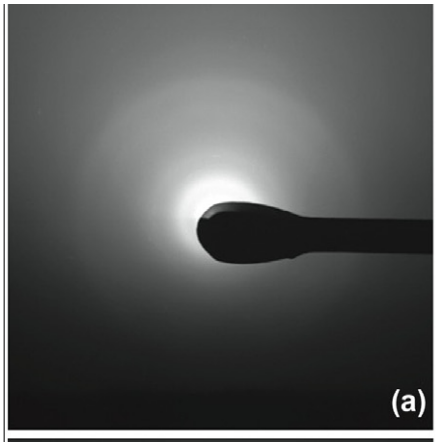

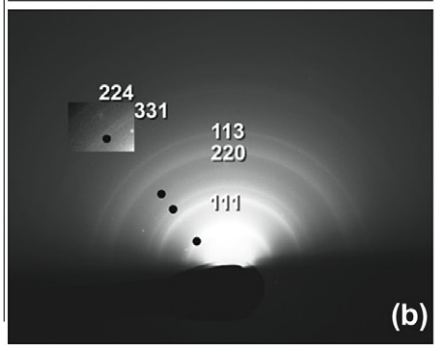

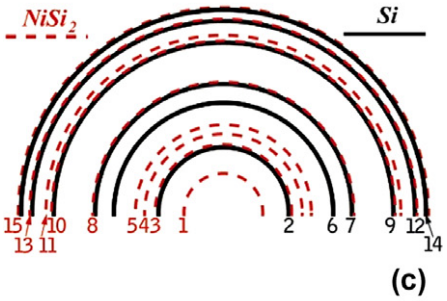

N_{Rings}	Measured	$NiSi_2$ Ref. 18		Si Fd-3m(227) (PDF 026-1481)	
	d(nm) ±0.001	hkl	d(nm)	hkl	d(nm)
1	0.539	100	0.540		
2	0.314			111	0.314
3	0.311	111	0.312		
4	0.269	200	0.270		
5	0.241	210	0.242		
6	0.192			220	0.192
7-8	0.164	311	0.163	311	0.164
9-10	0.125	331	0.124	331	0.124
11	0.119	420	0.120		
12-13	0.111	442	0.110	422	0.110
14-15	0.105	511	0.104	511	0.104

(d)

Figure 3. (a) Electron diffraction pattern from the outermost layers of an as-grown deposit obtained under condition II. The pattern was taken using the typical geometry of RHEED investigation in which the e-beam direction is glancing to the sample surface. In such conditions and considering the 3D morphology of the sample, the analysis gives a Transmission Electron Diffraction (TED) pattern through the protruding structures imaged in Figure 2d. The diffraction features suggest the concurrent presence of SWCNTs and MWCNTs. (b) RHEED pattern from the substrate surface after C-nanotubes removal; (c) schematic representation of the $NiSi_2$ (red dashed line) and Si (black line) Debye's rings revealed by the indexing and analysis of experimental pattern reported in a); (d) measured interplanar spacings and corresponding reference data for Si (PDF card #027–1402) and $NiSi_2$ [18]. (For interpretation of the references to color in this figure legend, the reader is referred to the web version of this article.)

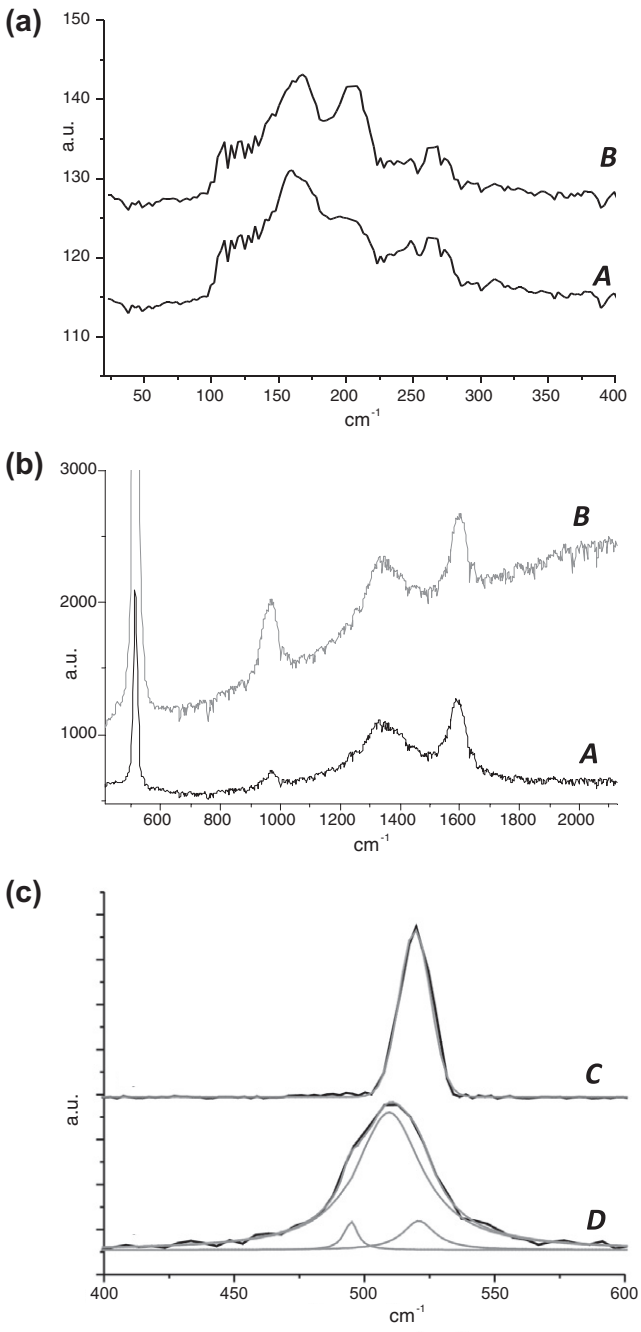

Figure 4. (a) Raman spectra in the RBM (Radial Breathing Mode) spectral range, from deposits obtained under condition I (spectrum A) and condition II (spectrum B). (b) Raman spectra taken in the spectral region of 400–2000 cm^{-1} using the 600 gr/mm grating, from deposits obtained under condition I (spectrum A) and condition II (spectrum B). (c) Raman spectra taken in the spectral region of 400–600 cm^{-1} using the 1800 gr/mm, in which is located the first-order scattering from Si. Spectrum C refers to the as-received uncoated Si (1 0 0) substrate, spectrum D to the sample grown under condition II.

The Raman spectroscopy is indeed a useful and reliable characterization tool able to reveal the crystalline state of semiconducting materials and to distinguish different Si structures [21,25,26].

Besides that, the analysis of one phonon Raman spectrum of Si nanostructures (particles and wires) is an intriguing matter of debate because of the discrepancies between the expected and measured spectra line-shapes. Different causes have been suggested for the inconsistency of the Raman parameters measured in nano-sized-Si. The one phonon Raman line shape has been found to be

modified by several factors [27–31], as sample inhomogeneity, Fano-scattering from photo generated carriers, stresses, and laser induced heating. In such a context, we specifically analyzed the spectral region where is located the first-order Raman signal of Si (400–600 cm^{-1}). Figure 4c reports on the comparison of the Si signals taken from the as-received uncoated single crystal Si (100) substrate (spectrum C) and from the sample grown under condition II (spectrum D). The used Si substrate exhibits a Gaussian lineshape with a maximum at ω = 518 cm^{-1} and a FWHM of 10 cm^{-1}. The slight red shift and the broadening of the Si band, with respect to the typical feature of Raman signal from single crystal Si (ω = 520 cm^{-1} and FWHM = 3 cm^{-1}), are consistent with a heating effect [32].

The spectrum from the sample grown under condition II (spectrum D) exhibits a larger downshift and an asymmetrical enlargement of the band. This curve can be deconvolved in three components located at about 480, 510, and 518 cm^{-1} that can be attributed to different Si states in the sample.

The shoulder at 480 cm^{-1} is due to the Raman peak generally attributed to amorphous Si [25–26].

The principal Raman signal centered at about 510 cm^{-1} has often been attributed to the first-order Raman frequency in Si nanostructures, and this signal shift, with respect to that one of the Si bulk, has been sometimes related to confinement effects. As a consequence, attempts were made to extrapolate the nanocrystallites size from this Raman signal shift, although [25–26] a shift more than 1 cm^{-1} is in contrast with the confinement theoretical prediction and seems rather related to laser heating effects coupled with a poor thermal dissipation.

Overall, the Si nanostructures, compared to bulk Si, seem to be extremely sensitive to very low temperature rising in terms of Raman signal thermal shift. Kostantinovic et al. [33] rationalized the detected Raman shift, induced by a low temperature increase due to a laser irradiation at low power, also on the base of a poor thermal contact with the substrate.

The position peak at 518 cm^{-1} with FWHM = 12 cm^{-1} is practically the same shown by as-received Si substrate (spectrum C).

Two different ultrasound–based treatments were carried out to prepare different series of TEM samples, with the aim to investigate the external and in-depth morphology of the samples produced under condition II. The first treatment was used to detach the elongated objects depicted in Figure 2c–d from the substrate; the second treatment, stronger and longer in time, was used to separate the outermost C-nanotubes deposits from the underlying 3D structures.

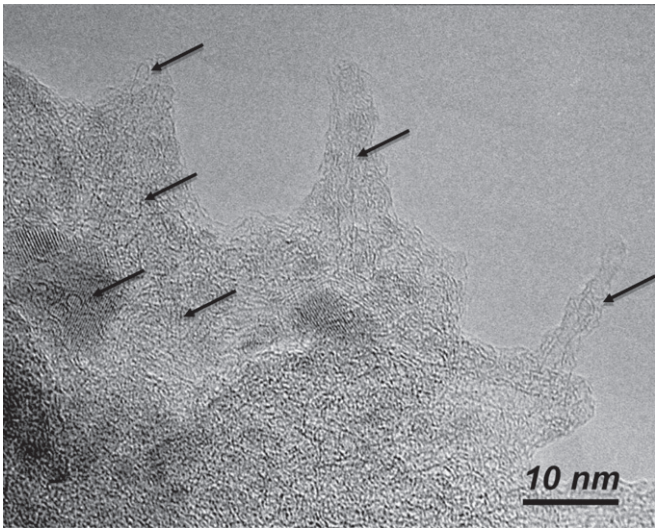

Figure 5. A typical HRTEM image of the outermost part of the vertical structures imaged in Figure 3c–d, after detachment from the substrate. The black arrows evidence individual SWCNTs.

A typical HR-TEM image of the outermost deposit is reported in Figure 5, in which arrows indicate some isolated SWCNT with different orientation protruding from the entangled C-nanotubes deposit.

An insight into the nature of the inner architectures supporting the C-nanotubes deposits has been achieved by combining Transmission Electron Microscopy (TEM) and Electron Diffraction (TED).

TEM micrographs of Figure 6a and b show the upper part of the frames underlying the C-nanotubes mats and evidence the peculiar morphology of the apical part of such frames. All the observed samples show two common characteristics:

(I) The presence of relatively large conical or quasi-cylindrical structures, that can be considered on the whole as truncated cones having different aperture angles, 2θ, and small base with different radius, *a*. Low θ values, combined with relatively large values of the radius, *a*, of the small base, correspond to cylindrical-like shapes: see Figure 6a for an example, in which $\theta \approx 5.5^{\circ}$ and $a \approx 50$ nm. Higher θ values, with very low values of the radius *a* of the small base, give conical-like shapes: see Figure 6b for an example, in which $\theta \approx 21^{\circ}$ and $a \approx 0$ nm.

(II) The multi-apex morphology of the apical part of such structures is characterized by a variable number of cuspidal features with different local density (from that of Fig 6a, representative of the lowest one, to those of Figure 6b, representative of highest one).

Overall, the multi-cusps arrangement produced on the apical part of the conical/cylindrical structures could likely offer an anemone-like support for the layout of nanotube mats.

The TED pattern in Figure 6c was produced, in selected area (SA) condition, from the same sample area imaged in Figure 6a. The indexing of its Debye's rings (Figure 6d) shows the predominant presence of polycrystalline Si nanosized, together with the typical haloes produced by the random scattering due to traces of amorphous material. Moreover, the complete indexing of Debye's rings (Figure 6e) revealed the presence of a second polycrystalline phase nanosized that has been identified as $NiSi_2$, in full agreement with the above reported analysis of RHEED pattern. The relative lower diffraction intensities due to the silicide, in comparison with those one corresponding to Si, confirmed, in agreement with the RHEED analysis, the presence of a very thin silicide layer, produced during the CVD process.

In some cases, the presence of diffraction rings related to a graphitic phase has also been detected. This occurrence can be explained by considering that it is very likely that the sample preparation method for TEM/TED analysis has not been able to detach all the C-nanotubes from the conical structures observed by FE–SEM (Figs. 2c–d).

Overall, the reported data strongly indicate that the conical/cylindrical forms generated under condition II have a nanocrystalline Si core shaped as elongated structures ending with narrow multi-cusps, and are coated by mats of C-nanotubes grown over the supporting Si frames. Differently from other hybrid C/Si structures [1–2] requiring multi-steps processes for their fabrication, these C- and Si-based entities are generated during a kinetically driven single-step deposition process.

A possible model of the growth mechanism of conical/cylindrical Si nanostructures from Si substrates may be suggested on the basis of the following steps. A schematic of the proposed growth mechanism is reported in Figure 7.

At the onset of the process the substrate is heated up to 500 °C (Figure 7a); afterward the plasma is activated and the substrate starts to be biased. The negative biasing induces a translation of the MW plasma and a MW-RF capacitive coupling occurs close to

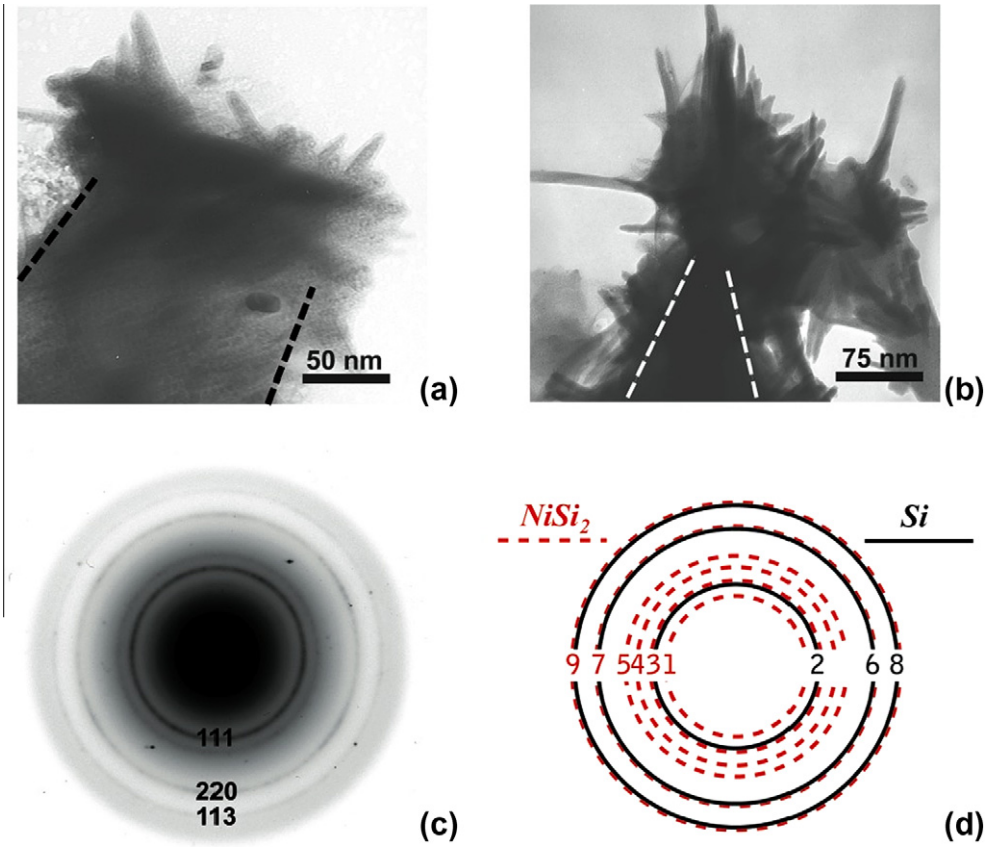

N_{Rings}	Measured	$NiSi_2$ Ref. 18		Si Fd-3m(227) (PDF 026-1481)	
	d(nm) ±0.001	hkl	d(nm)	hkl	d(nm)
1	**0.380**	110	0.381		
2	**0.314**			111	0.314
3	**0.311**	111	0.312		
4	**0.269**	200	0.270		
5	**0.241**	210	0.242		
6-7	**0.192**	220	0.191	220	0.192
8-9	**0.164**	311	0.163	311	0.164

(e)

Figure 6. (a–b) TEM images of two representative apical parts of the frames underlying the C-nanotubes mats, from samples obtained after a prolonged sonication, able to separate and disperse the external C-nanotubes. All observed apical parts are characterized by the presence of a variable density of cusps, from a very low local density (a) to a relatively high density (b). The dashed lines put in evidence the underlying vertical structures: with a quasi-cylindrical shape (black dashed lines in a) and with a quasi-cylindrical shape in (white dashed lines in b). (c) Transmission Electron Diffraction (TED) pattern taken from the area imaged in (b). The pattern substantially coincides with the one achieved from the area imaged in (a), not reported for sake of brevity. (d) Schematic representation of the $NiSi_2$ (red dashed line) and Si (black line) Debye's rings revealed by the indexing and analysis of experimental pattern reported in (a). (e) Measured interplanar spacings and corresponding reference data for Si (PDF card #027–1402) and $NiSi_2$ [18]. (For interpretation of the references to color in this figure legend, the reader is referred to the web version of this article.)

the substrate. If the self-bias is high (above approximately 200 V) the combined effects of the substrate heating and of the energetic H ion bombardment facilitate the Si diffusion inside Ni (and vice versa) [34] and generate a molten Si/Ni phase rich in Si (Figure 7b). This phase, similar to the whole Si substrate, is negatively polarized and feels the average electrical field between substrate and plasma. In this field, the Si/Ni molten phase, differently from the solid substrate, is subjected to a vertical translation and is pulled upward along the lines of the electric field. This interaction gives rise to the formation of the elongated Si nanostructures (Figure 7c). At the same time the Ni present on these narrow Si cones acts as catalyst for the synthesis of carbon nanotubes that begin to grow by taking advantage of the gas inlet in the vicinity of the Si tops that produces a hyper concentration of carbon atoms and clusters. The dense coverage of C-nanotubes observed on the tips of the Si cones can be explained considering that the tops encounter a larger spherical angle of the gas phase with respect to the walls. This increases the probability that active species reach the top of the cones, compared with that for the bottom regions at the base of the cones.

At the end of the process, after plasma switching off, the rapid cooling induces a rapid re-crystallization of the Si in nanocrystalline structures and the formation of a very thin layer of $NiSi_2$ that remain coated by the C-nanotubes deposits (Figure 7d). This mech-

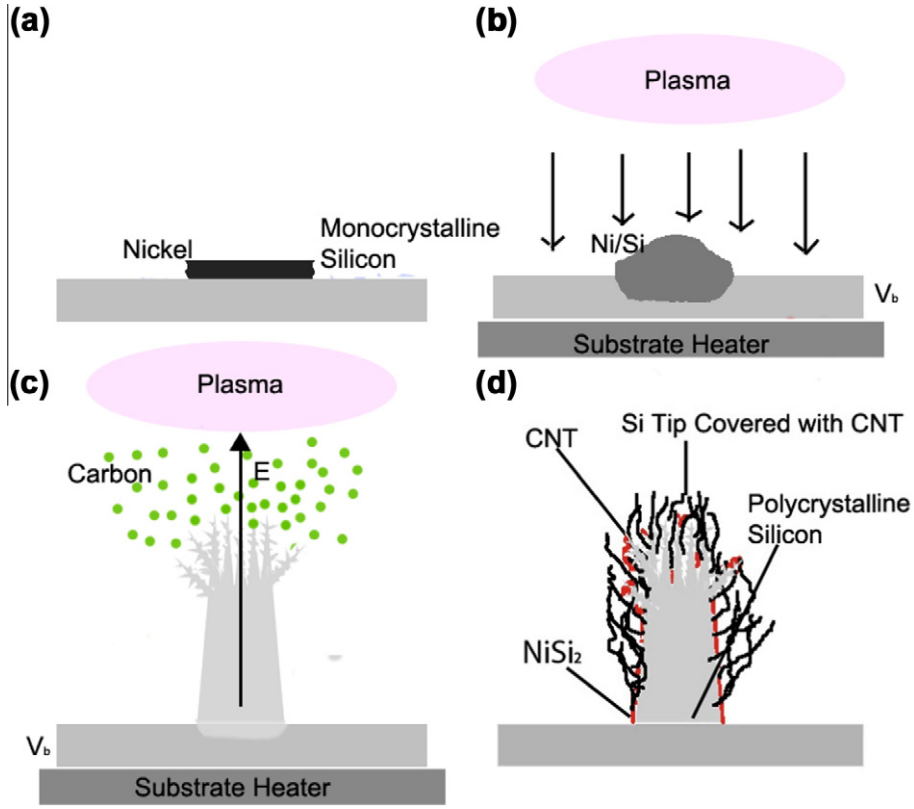

Figure 7. A schematic drawing of the proposed mechanism for the one-step growth of Si nanocones coated by C-nanotubes: (a) Si substrate with Ni catalyst; (b) formation of a molten Si/Ni phase due to combined effects of substrate heating and energetic H ion bombardment; (c) vertical translation and pulling up of the Si/Ni molten phase along the lines of the electrical field (E); (d) Ni- catalyzed growth of carbon nanotubes onto the rising elongated Si nanostructures covered by a very thin layer of $NiSi_2$.

anism would explain why the Si nanostructures are produced only in the presence of high biasing, whereas lower values of bias enable to deposit only C-nanotubes.

In this context the role played by the Ni layer deposited on the Si substrate would not only catalyze the synthesis of C-nanotubes onto Si elongated frames, but also lower the melting temperature of the substrate, due to the formation of Si/Ni systems under surface heating and activation via intense ion bombardment. This hypothesis is confirmed by some experiments carried out under the same conditions, but on substrates prepared in different ways.

In Figure 8 are reported the FE-SEM images of samples grown using condition II on two kinds of substrates patterned by lithography with spots of 150 nm diameter. The image of Figure 8a shows a conical structure vertically grown on a 150 nm Ni spot in direct contact with the Si substrate. The image of Figure 8b shows the material obtained by depositing 15 nm of TiN as anti-diffusion interlayer between the Si substrate and the 150 nm Ni spot. In this last case no aligned vertical structures are produced and the deposit is similar to those obtained from runs carried out under condition I, i.e. bush-like ensembles of C-nanotubes bundles. It is also evident, by the comparison of Figure 8a and Figure 8b, that the Ni spot does not undergo significant changes in the presence of a thin TiN interlayer (Figure 8b), while it is practically dissolved in case of absence of such interlayer (Figure 8a).

The results of these last experiments indicate that the TiN interlayer acts effectively as a barrier blocking the diffusion of Si into the Ni layer, and that the mechanism of nanostructure growth in the presence of anti-diffusion TiN interlayer is no longer dependent on the self-bias.

4. Conclusions

In the present study we have demonstrated that a dual mode microwave/radio frequency plasma system can be used in order to activate kinetically driven processes able to create new chemistries and to open unexpected routes for integration of Si and C elements in hybrid nanostructures.

The objective of the work described in this Letter was to assess the feasibility to produce innovative Si/C entities, to identify and optimize the growth conditions and to establish the experimental parameters for the reproducible fabrication of tipped Si nanocones coated by C-nanotubes. The one-step PE-CVD processes on highly biased (>200 V) Si substrates, with Ni-coated patterned areas, are able to generate two-component elongated structures.

The growth features of coupled cuspidated Si and tubular C components have been investigated by means of FE-SEM, TEM, micro- Raman scattering, RHEED and ED techniques, and the building of hybrid Si/C nanostructures has been related to dynamic coupling of MW and RF plasma.

Our results lead to the following main conclusions, taking into account that the biasing of the sample holder depends on both the RF power and the total pressure in the MW-RF reactor:

- The RF induced biasing plays a fundamental role in the growth of Si/C nanostructures, negatively polarizing the Si substrate and addressing the synthesis towards different pathways;
- On Si substrates coated with Ni layers, the substrate heating and the bombardment of energetic H ions, provoked by high biasing, induce phase melting and diffusion of Si inside the Ni layer at the substrate surface;

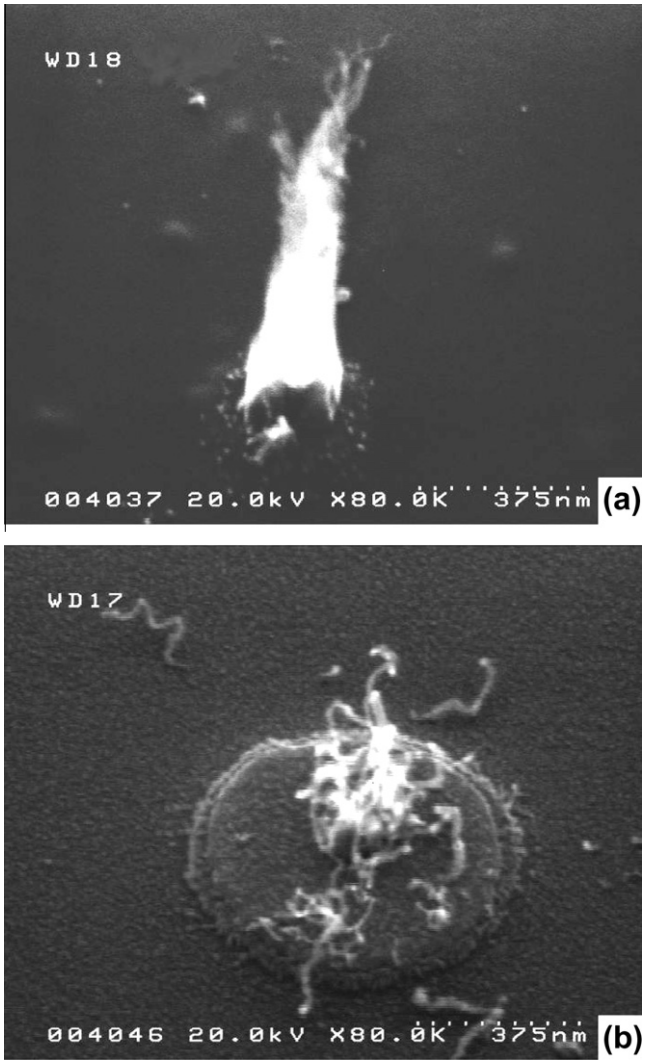

Figure 8. FE-SEM images of deposits produced under condition (II) on patterned Si substrates, prepared by: (a) sputtering Ni directly onto the 150 nm spot on the Si substrate; (b) sputtering Ni onto a 15 nm thick TiN layer deposited on the 150 nm spot on Si substrate.

- Under the exposure to the electrical field, the molten Si/Ni phase is pulled up along the vertical field lines, producing narrow conical objects, whereas C-nanotubes begin to growth from the gas phase due to the presence of the Ni catalyst. At the end of process, a very thin layer of $NiSi_2$ remains as intermediate layer between the underlying Si and the outermost C-nanotube deposit.

This model, conceived to give a possible explanation of the concurrent growth of Si and C nanostructures, accounts for the production of elongated conical structures formed by a Si core and by an outermost deposit of entangled nanotube bundles.

Growth experiments have also been carried out under the same conditions on small areas (spots with a diameter of 150 nm) of substrates prepared following different methodologies. The aim was to better investigate the features of the deposits and to confirm the growth mechanism proposed for the C-nanotubes coated Si cones. By depositing a TiN interlayer between Si and Ni, we were able to prevent phase modifications of the Si surfaces leading to only C-nanotubes deposits and no Si cones being produced.

Overall, the results seem to show that a dynamic competition between the formation of Si and C-nanotubes takes place in PE-CVD reactors and that different reaction pathways can be opened under proper biasing conditions.

The fabrication of hybrid systems composed by different nanostructures based on C and Si represents a significant and yet still unexplored field of research, despite the relevant technological potentialities of such systems. Both development of MW-based careful growth strategies and engineering of such apparatuses are strongly needed for the optimization of already obtained nanostructures, as well as design of novel nanomaterials and widening of Si/C photonic, electronic and photovoltaic applications.

The recent general improvements in plasma nanotechnology [35,36] can represent a fundamental key and can help in the control and reproducibility of the features of carbon nanostructures [37,38], as required by the technological exploitation of hybrid C-nanotubes/Si 3D nanostructures, in the framework of the above reported applications.

Acknowledgements

This Letter has been partially supported by the Italian MIUR through the PRIN2008 project: '*Advanced nanomaterials and nanostructures for field- and photo-emission based devices*'.

Many thanks to prof. Daniela Manno for helpful discussion and HRTEM image.

References

[1] Y. Cui, Z. Zhong, D. Wang, W.U. Wang, C.M. Lieber, Nanoletters 3 (2003) 149.
[2] W. Wang, P.N. Kumta, ACS Nano 4 (2010) 2233.
[3] J.R. Petta et al., Science 309 (2005) 2180.
[4] N. Mason, M.J. Biercuk, C.M. Marcus, Science 303 (2004) 655.
[5] M. Liu, G. Lu, J. Chen, Nanotechnology 19 (2008) 265705.
[6] M.L. Terranova, V. Sessa, M. Rossi, CVD 12 (2006) 315.
[7] M.L. Terranova, S. Orlanducci, A. Fiori, E. Tamburri, V. Sessa, M. Rossi, A.S. Barnard, Chem. Mat. 17 (2005) 3214.
[8] S. Orlanducci, E. Tamburri, M.L. Terranova, M. Rossi, CVD 14 (2008) 241.
[9] H. Shirai, T. Kobayashi, Y. Hasegawa, Appl. Phys. Lett. 87 (2005) 143112.
[10] Z. Yang, H. Shirai, T. Kobayashi, Y. Hasegawa, Thin Solid Films 515 (2007) 4153.
[11] R. Etemadi et al., J. Vac. Sci. Technol., A 15 (1997) 320.
[12] R. Etemadi, C. Godet, J. Perrin, Plasma Sources Sci. Technol. 6 (1997) 323.
[13] R. Etemadi, C. Godet, J. Perrin, A. Seignac, D. Ballutaud, J. Appl. Phys. 83 (1998) 5224.
[14] L. Martinu, D. Poitras, J. Vac. Sci. Technol., A 18 (2000) 2619.
[15] W. Kaczorowski, P. Niedzielski, Adv. Eng. Mater. 10 (2008) 651.
[16] M. Rossi, G. Vitali, D. Karpuzov, H. Budinov, M. Kalitzova, J. Mater. Sci. 26 (1991) 3337.
[17] M.L. Terranova, S. Piccirillo, V. Sessa, P. Sbornicchia, M. Rossi, S. Botti, D. Manno, Chem. Phys. Lett. 32 (2000) 284.
[18] W.B. Pearson, Handbook of Lattice Spacing and Structures of Metals and Alloys, Pergamon, New York, 1958.
[19] W.B. Pearson, The Crystal Chemistry and Physics of Metals and Alloys, Wiley, New York, 1972.
[20] A. Franciosi, J.H. Weaver, F.A. Schmidt, Phys. Rev. B 26 (1982) 546.
[21] P.A. Temple, C.E. Hathaway, Phys. Rev. B 7 (1973) 3685.
[22] M.A. Pimenta, G. Dresselhaus, M.S. Dresselhaus, L.G. Can cado, A. Jorio, R. Saito, Phys. Chem. Chem. Phys. 9 (2007) 1276.
[23] M.A. Tamor, W.C. Vassel, J. Appl. Phys. 76 (1994) 3823.
[24] Z.L. Tzakadze, K. Ostrikov, J.D. Long, S. Xu, Diam. Rel. Mater. 13 (2004) 1923.
[25] H. Richter, Z.P. Wang, L. Ley, Solid State Commun. 39 (1981) 625.
[26] I.H. Campbell, P.M. Fauchet, Solid State Commun. 58 (1986) 739.
[27] Y. Cui, C. Lieber, Science 291 (2001) 851.
[28] S. Bhattacharyya, S. Samui, Appl. Phys. Lett. 84 (2004) 1564.
[29] R. Gupta, Q. Xiong, C.K. Adu, U.J. Kim, P.C. Eklund, Nano Lett. 3 (2003) 627.
[30] S. Piscanec et al., Phys. Rev. B 68 (2003) 241312R.
[31] K.W. Adu, H.R. Gutiérrez, U.J. Kim, P.C. Eklund, Phys. Rev. B 73 (2006) 155333.
[32] M. Balkanski, F. Wallis, E. Haro, Phys. Rev. B 28 (1983) 1928.
[33] M.J. Konstantinović, S. Bersier, X. Wang, M. Hayne, P. Lievens, R.E. Silverans, V.V. Moshchalkov, Phys. Rev. B 66 (2002) 161311.
[34] W.-S. Lee, T.-H. Chen, C-F. Lin, J-M. Chen, Appl. Phys. A 100 (2010) 1089.
[35] K. Ostrikov, U. Cvelbar, A.B. Murphy, J. Phys. D: Appl. Phys. 44 (2011) 174001.
[36] M. Meyyappan, J. Phys. D: Appl. Phys. 44 (2011) 174002.
[37] R.M. Sankaran, J. Phys. D: Appl. Phys. 44 (2011) 174005.
[38] M. Keidar, A. Shashurin, J. Li, O. Volotskova, M. Kundrapu, T.S. Zhuang, J. Phys. D: Appl. Phys. 44 (2011) 174006.